# We are IntechOpen, the world's leading publisher of Open Access books Built by scientists, for scientists

**4,800**
Open access books available

**122,000**
International authors and editors

**135M**
Downloads

Our authors are among the

**154**
Countries delivered to

**TOP 1%**
most cited scientists

**12.2%**
Contributors from top 500 universities

CLARIVATE ANALYTICS BOOK CITATION INDEX INDEXED

WEB OF SCIENCE™

Selection of our books indexed in the Book Citation Index in Web of Science™ Core Collection (BKCI)

## Interested in publishing with us?
## Contact book.department@intechopen.com

Numbers displayed above are based on latest data collected.
For more information visit www.intechopen.com

# 26

# Anomalous Transient Photocurrent

Laigui Hu[1] and Kunio Awaga[2]
[1]*Department of Applied Physics, Zhejiang University of Technology,*
[2]*Department of Chemistry and Research Center for Materials Science, Nagoya University,*
[1]*China*
[2]*Japan*

## 1. Introduction

The operating principle in conventional optoelectronic devices is based on steady-state photocurrent. In these devices, photogenerated carriers have to travel long distances across the devices. Various dissipation mechanisms such as traps, scattering and recombination dissipate these carriers during transport, and decrease device response speed as well as optoelectronic conversion efficiency, especially in organic devices (Forrest & Thompson, 2007; Pandey et al., 2008; Saragi et al., 2007; Spanggaard & Krebs, 2004; Xue, 2010). Such organic devices have received considerable attention due to their potential for of large-area fabrication, combined with flexibility, low cost (Blanchet et al., 2003), and so on. Efforts to substitute inorganic materials by organic ones in optoelectronics have encountered a serious obstacle, i.e., poor carrier mobility that prevents photogenerated carriers from travelling a long distance across the devices.

Typically, exciton diffusion length in organic materials is approximately 10-20 nm (Gunes et al., 2007). Internal quantum efficiency decreases with the increase in film thickness (Slooff et al., 2007) since recombination will occur prior to exciton dissociation if photogenerated excitons are unable to reach the region near the electrodes. Therefore, though a thicker film can result in an enhanced light harvesting, collecting carriers using electrodes becomes difficult. In addition, the poor mobility of organic materials always triggers the formation of space charges in thin film devices, and the space charges additionally limit the photocurrent (Mihailetchi et al., 2005).

In this chapter, we introduce an anomalous transient photocurrent into optoelectronics based on Maxwell's theory on total current, which consists of conduction and displacement current. In contrast to organic optoelectronic devices based on conduction photocurrent, which sufferrs from poor carrier mobility, the anomalous photocurrent can contribute to optoelectronic conversion and "pass" through an insulator. Though such anomalous photocurrent, or photoinduced displacement current, has received previous attention (Andriesh et al., 1983; Chakraborty & Mallik, 2009; Iwamoto, 1996; Kumar et al., 1987; Sugimura et al., 1989; Tahira & Kao, 1985), its mechanism and characteristics are still largely unresolved. We systematically explained this phenomenon based on our theoretic analyses and experiments on an organic radical 4'4-bis(1,2,3,5-dithiadiazolyl) (BDTDA) (Bryan et al., 1996) thin film device. A double-layer model was introduced, and a new type of device with structure of metal/blocking layer/semiconductor layer/metal was developed to reproduce the anomalous photocurrent (Hu et al., 2010b). The photocurrent transient is observed to

involve polarisation in the materials, and stored charges within the phtocells can be released by the time-dependent conduction photocurrent. The formulae derived for this phenomena are promising for the characterisation of carrier transport in organic thin films.
In this chapter, we firstly demonstrate the anomalous photocurrent and steady-state photocurrent in the BDTDA photocells with a structure of ITO/BDTDA (300 nm)/Al (Hu et al., 2010a; Iwasaki et al., 2009). The anomalous photocurrent in the BDTDA films is observed to involve a large polarisation current induced by the formation of space charges near the electrodes. Subsequently, a series of formulae based on the total current equation for a double-layer system have been developed to fit experimental data. The theoretical ideas behind this formula are discussed as well.
Based on the analyses, the metal/blocking layer/semiconductor layer/metal photocell is demonstrated using different organic materials, including insulators and semiconductors, to reproduce the anomalous photocurrent. We introduce the enhancement of anomalous photocurrent by employing a transparent dielectric polymer with a larger dielectric constant (as a blocking layer) since larger polarisation current can be produced. Fast speed can be achieved since the performance is mainly limited by the fast dielectric relaxation (Kao, 2004). These are promising for high-speed operation in optoelectronics. Afterward, the properties of anomalous photocurrent, including light intensity dependencies, are demonstrated.
Finally, we briefly introduce a new method for mobility measurements based on the double-layer model. Unlike the time of flight technique and field effect transistor measurements, this method can be used for an ultra-thin organic semiconductor to check carrier transport along the directions perpendicular to electrodes in photocells. Furthermore, we demonstrate that the technique can be utilised to check the dominant carrier types in a semiconductor. The final section includes the summary and proposals.

## 2. Anomalous photocurrent in BDTDA photocells

Anomalous transient photocurrent has been independently revealed in organic materials and amorphous inorganic materials. In extant literatures, mechanisms such as trapping/detrapping or electron injection from electrodes were adopted to interpret this behaviour in different materials. A common understanding from previous reports is that the transient photocurrent comes from organic or amorphous materials with poor carrier mobility or large thickness. However, the effects of the dielectric properties on related materials were seldom studied in detail. Moreover, we observed the anomalous transient photocurrent in a radical BDTDA thin film device with a significant imbalance of carrier transports. As a model material, behaviour in the BDTDA devices will be introduced in this section, as well as the physical properties of the pink BDTDA thin films.

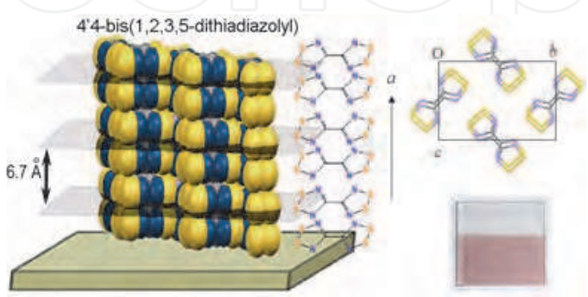


Fig. 1. Molecular π-stacking along the monoclinic *a* axis of BDTDA, a photograph of a thin film on ITO, and the molecular packing in the *bc* plane for this material

### 2.1 Characteristics of BDTDA thin films

#### 2.1.1 Film structures

BDTDA is a disjoint diradical. Molecular orbitals for the two unpaired electrons are localised to separate five-membered rings, and exchange interactions between the two radical centres are very small. Its crystal structure consists of a face-to-face BDTDA dimer, indicating that intermolecular interaction is stronger than intradimer interaction. These dimers show π-stacking along the monoclinic *a* axis. Packing of dimeric stacks produces a herringbone-like motif with electrostatic $S^{\delta+}\ldots N^{\delta-}$ contacts, in which all the molecular planes of BDTDA are parallel to the *bc* plane. It is notable that BDTDA films consist of alternating 1-dimensional π-stacking with molecular planes parallel to the substrates, as shown in Fig. 1 (Iwasaki et al., 2009; Kanai et al., 2009). Therefore, π-stacking can bridge the distance between bottom and top electrodes, which aids photoconduction between the electrodes.

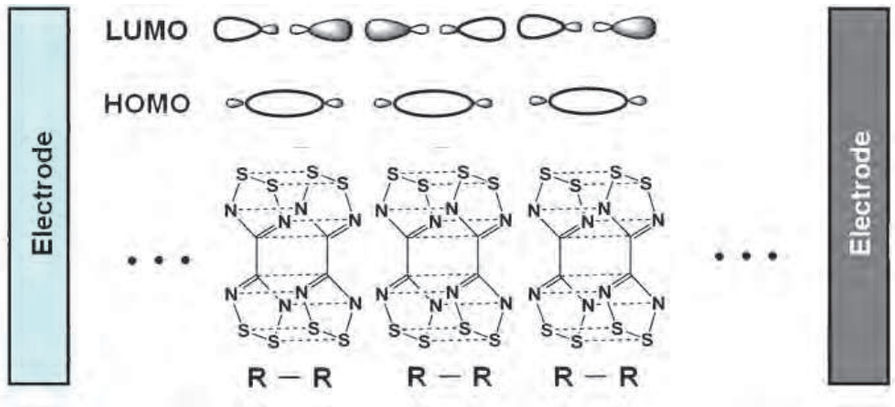


Fig. 2. Bonding and antibonding supramolecular orbitals of π–radical dimer.

#### 2.1.2 Imbalance of carrier transport in BDTDA films

Considering that two π-radical BDTDA molecules exhibit face-to-face overlap, a bonding supramolecular orbital and an antibonding supramolecular orbital are developed (Fig. 2). The population of the bonding supramolecular orbital is concentrated at the centre of the dimer, while that of the antibonding supramolecular orbital spreads outside along the R—R axis. Since these radical dimers create stacking chains with π-π interactions, the antibonding supramolecular orbitals are expected to form a wide band through a large interdimer overlap; population of the lowest unoccupied molecular orbital (LUMO) spreads towards the outside of the dimer. By contrast, the highest occupied molecular orbital (HOMO) forms a narrow band. Therefore, a significant imbalance of carrier transport can be expected, specifically high photoconductivity by the electron migration in the wide LUMO band and poor hole mobility in the narrow HOMO band. In addition, the valence bond image (Iwasaki et al., 2009) suggests that the photoexcited state includes a character of charge transfer, namely, $R{:}R \rightarrow R^{+}R^{-}$, where R is a radical. In other words, electrons will be directly promoted from one molecule to another by photons, which can be regarded as a precursor stage of charge separation. These characteristics are promising for developing photoactivities.

#### 2.1.3 Space charge limited current in BDTDA films

To characterise the diradical film, photocells with a structure of ITO/BDTDA (300 nm) /Al were prepared (Fig. 3) and current-voltage (*J-V*) characteristics were recorded. BDTDA was

prepared as described in a previous report (Bryan et al., 1996), and was thermally evaporated onto ITO glasses. As a top electrode, Al was also thermally evaporated onto the thin films. The effective area of this photocell was approximately 0.02 $cm^2$. The sample was then fixed into a cryostat with a pressure below 1 Pa. During measurement, the Al electrode was grounded, and bias polarity was defined as plus when a positive bias voltage was applied to ITO.

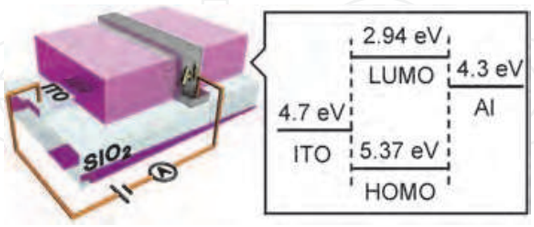


Fig. 3. Schematic views and an energy diagram of BDTDA photocells.

*J-V* characteristics were investigated using a picoammeter/voltage source under dark conditions and the bias voltage was scanned from -3 V to 3V. As shown in Fig. 4(a), the *J-V* curve exhibits a rectification behaviour, and rectification rate is approximately $10^2$ at ±2 V. This behaviour is reasonable, as the work functions of the two electrodes are different, and non-injecting (see energy diagram of electrodes and BDTDA in the inset of Fig. 3). The applied bias $V$ was corrected (van Duren et al., 2003) to compensate for the built-in voltage ($V_{bi} \approx 0.4$ V) that arises from work function difference between the two electrodes. Voltage drop across the series resistance of BDTDA devices was ignored, as its value was negligibly small.

Figure 4(b) exhibits the log ($J$)-log ($V$) plots for the data in Fig. 4(a). This curve consists of two regions with a crossover point at ~0.8 V, below which the *J-V* curve demonstrates Shockley behaviour that is ascribed to the injection limited current. At higher voltages (V > 0.8 V), the *J-V* curve shows a linear dependence, and its slope can be estimated as ~4.9. This value indicates that space charge limited current dominates the curve, though the dependence does not satisfy Child's law ($J \propto V^2$) (Coropceanu et al., 2007; Karl, 2003). This is a bulk limited current ascribed to a trap-controlled space charge limited current or a space charge limited current with a field dependence of carrier mobility (Blom et al., 1997; Sharma, 1995). Therefore, space charges are easily generated in this thin film devices, mainly due to significant imbalance of carrier transport and relatively large thickness (300 nm).

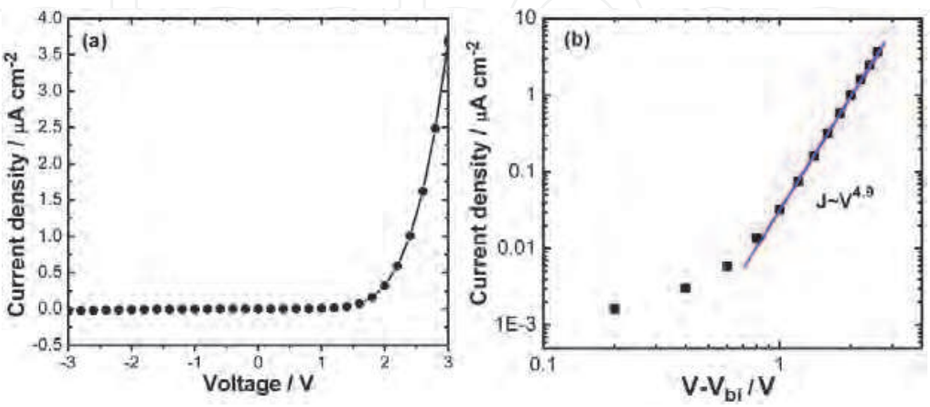


Fig. 4. *J-V* characteristics of a BDTDA photocell under a dark condition; (a) linear plot of $J$ versus $V$; (b) log ($J$)-log($V$) plot for the data in (a).

### 2.2 Photoresponses of BDTDA films

To measure the photocurrent of the photocells, a monochromated light, and green laser (532 nm) that can produce a stronger illumination, were employed as light source to irradiate the samples. To match the absorption band of BDTDA thin films, light with a wavelength of 560 nm was chosen for weak illumination to the transparent ITO electrode. We adopted lock-in techniques or an AC method (Ito et al., 2008) for normalised photocurrent-action spectra.

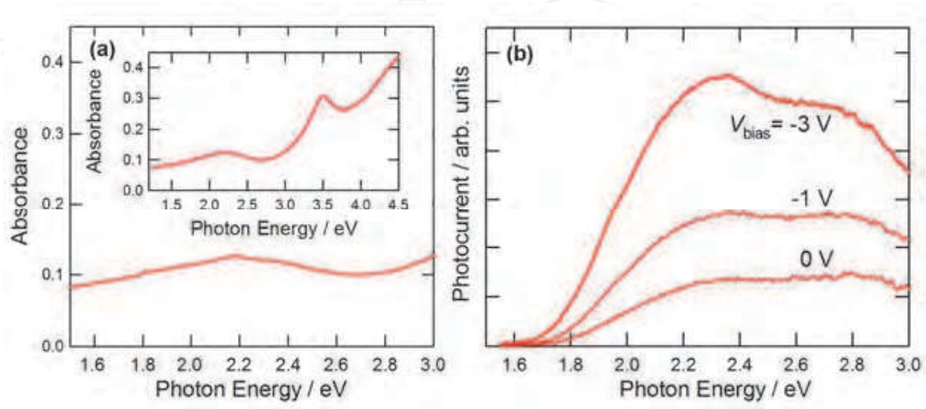


Fig. 5. (a) Absorption spectrum of BDTDA thin film; the inset shows the whole data within the range of 1.4-4.5 eV; (b) photocurrent-action spectra

#### 2.2.1 Steady-state photocurrent of BDTDA films

To determine the optical properties of BDTDA thin films for photocurrent measurements, absorption spectrum of the BDTDA thin film (100 nm) on a quartz substrate within the range of 1.5-3.0 eV was recorded, as shown in Fig. 5(a). The inset shows data in the whole range of 1.2-4.5 eV. It is notable that there is a broad band around 2.1 eV that covers the whole visible range. The molecular orbital calculations indicate that this broad band is a complex of various electronic transitions, including intramolecular-, intradimer-, and interdimer transitions, allowed in the dimeric structure of this disjoint diradical. Subsequently, we examined the photoresponse of ITO/BDTDA (300 nm)/Al sandwich-type photocells.

Figure 5(b) shows the plots of photocurrent versus the photon energy (photocurrent-action spectra) measured by a lock-in technique with bias voltages $V_{bias}$= -3, -1 and 0 V. Photocurrent is obtained in the whole range of visible light (1.8-3.0 eV), while it shows a quick decrease below 2.2 eV. This decrease is possibly caused by the fact that absorptions below this energy are due to intramolecular excitations. The wide-range response, shown in Fig. 5(b), is advantageous for practical application as photodetectors.

Figure 6 is the photocurrent induced by green laser light illuminating from the ITO side with a small reverse bias voltage $V_{bias}$ of -3V. Upon illumination, conductivity is enhanced with an on/off gain of $1.8\times10^2$ under an excitation light intensity of 1.59 mW/cm$^2$. The corresponding photoresponsivity ($R_{res}$) was calculated to be approximately 3.5 mA/W based on the relation $R_{res} = (I_{ph})/IA$, where $A$ is the effective device area; $I_{ph}$ and $I$ are the photocurrent and the incident light intensity, respectively. The on/off ratio increases with the light intensity, and its maximum value observed in our experiments is approximately $10^3$. Meanwhile, the photoresponsivity demonstrates an inverse behaviour, and changes from $10^{-1}$ to $10^{-4}$ A/W, which is comparable to that of the most advanced organic polymer photodetectors for visible region (Hamilton & Kanicki, 2004; Narayan & Singh, 1999; O'Brien et al., 2006; Xu et al., 2004).

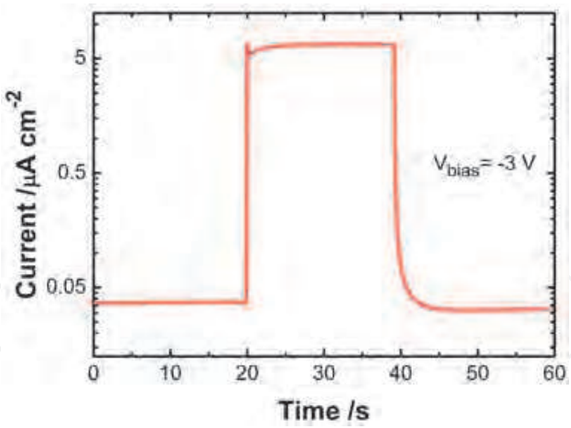


Fig. 6. On/off switching properties of the BDTDA photocell.

It is notable that the ITO/BDTDA/Al cells produce a photocurrent even at $V_{bias}$= 0 V, due to the potential difference of the electrodes, specifically ITO (4.8 eV) and Al (4.3 eV). This photovoltaic behaviour is consistent with the energy scheme in Fig. 3 taken by UPS/IPES measurements (Iwasaki et al., 2009). It is possible that the charge separation character in the photoexcited state, namely R+R-, contributes to this photovoltaic behaviour.

### 2.2.2 Anomalous transient photocurrent of BDTDA films

Figure 7(a) shows the photoresponses of an ITO/BDTDA/Al photocell with a bias voltage of 0 V. Upon illumination, a large anomalous transient photocurrent followed by a steady-state photocurrent was observed. Upon removal of illumination, a negative anomalous transient photocurrent was detected. Both the anomalous transient photocurrent and steady-state photocurrent increase with increases in light intensity. Figure 7(b) demonstrates the short circuit photoresponses under a reverse bias voltage of -2 V. Note that the anomalous transient photocurrent can be dramatically suppressed by applying a bias voltage. In particular, the negative current is nearly eliminated, while the steady-state current is increased. It is notable that anomalous transient photocurrent values under the zero bias can be comparable to those of the steady-state photocurrent under a bias voltage *V*. Positive anomalous transient photocurrent with weak excitation light intensity (≤ 0.57 μW/cm²) decreases exponentially with time, and decay time of the positive anomalous transient photocurrent shows light-intensity dependence. As shown in Fig. 7(a), a stronger illumination causes faster decay. Meanwhile, for the light intensity of > 0.57 μW/cm², positive anomalous transient photocurrent cannot fit well with a single exponential simulation. This indicates that anomalous transient photocurrent is a superposed signal with different mechanisms.

Quantum efficiencies for steady-state photocurrent and anomalous transient photocurrent were calculated by neglecting reflection losses at the device surfaces. Figure 8(a) shows the intenal quantum efficiency (Pettersson et al., 2001) versus photon energy plots for the peak values of the positive (red curve) and negative anomalous transient photocurrent (blue curve) and for steady-state photocurrent under monochromatic illumination with weak intensity from a halogen lamp. Intenal quantum efficiency values for the positive and negative anomalous transient photocurrent show increases with an increase in photon energy, and their values are considerably higher than that of the steady-state photocurrent (black curve). It is notable that the transient intenal quantum efficiency for the positive

anomalous transient photocurrent reaches an extremely high value of 65% at the photon energy of 2.8 eV, and its root mean square value is estimated to be ~30%; intenal quantum efficiency values of steady-state photocurrent are ~6%, corresponding to an external quantum efficiency of ~2%.

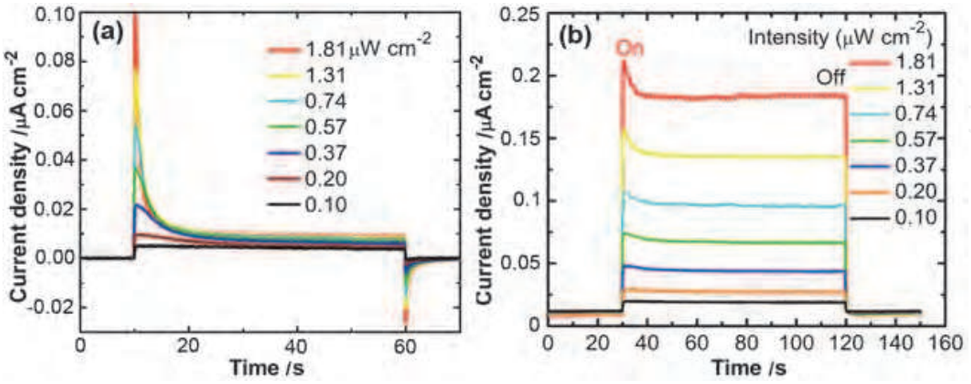


Fig. 7. Photoresponses of a BDTDA photocell with an illumination of 560 nm; (a) photoresponses under different light intensities with a zero bias voltage; (b) photoresponses under different light intensities with a bias voltage of -2 V.

To explore the recombination processes and mechanisms for anomalous transient photocurrent, we examined the light intensity dependence of the positive anomalous transient photocurrent and steady-state photocurrent. The results are shown in Fig. 8(b), where both axes are in a logarithmic scale. Both anomalous transient photocurrent and steady-state photocurrent obey a power law: $J \propto I^{\alpha}$, with $\alpha = 0.93$ for the former or $\alpha = 0.28$ for the latter. The former value suggests that monomolecular or geminate recombination (Binet et al., 1996) plays a role in the process. The latter α value suggests that the steady state suffers from higher order recombination processes, such as Auger (Wagner & Mandelis, 1996) and quadrimolecular recombinations (Marumoto et al., 2004). Considering that the α value is close to 0.25, quadrimolecular recombinations are more likely; adjacent photogenerated $R^+R^-$ pairs may interact with each other and recombine simultaneously.

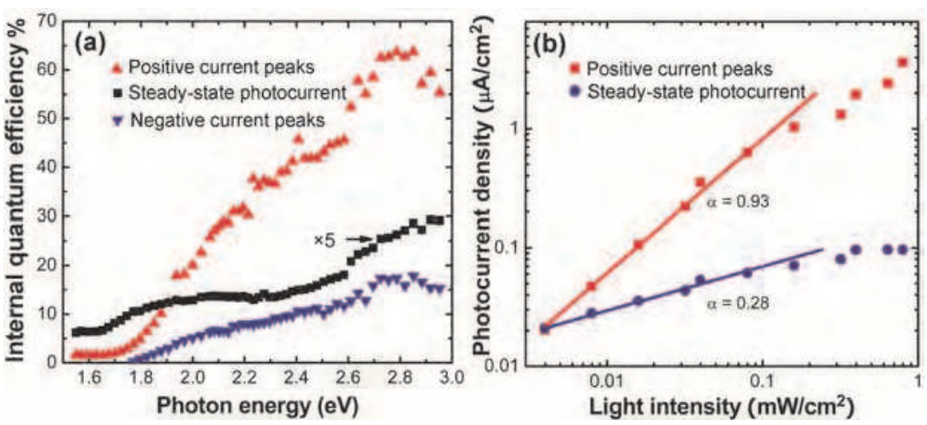


Fig. 8. (a) Intenal quantum efficiency values of the anomalous transient photocurrent and steady-state photocurrent for a BDTDA photocell; (b) light intensity dependence of the positive anomalous transient photocurrent (red points) and the steady-state photocurrent (blue points) induced by the green laser.

## 3. Mechanisms of anomalous photocurrent in BDTDA

Due to imbalance of carrier transports and the energy scheme of photocells, the junction at the Al/BDTDA interface plays the dominant role for the transient photoresponse (Hu et al., 2010a) if the BDTDA film is fully depleted. On the contrary, ITO/BDTDA with a larger barrier plays a main role if the film is not depleted. The junction acts as an active region (dark pink region in Fig. 9), which makes a different contribution to the anomalous transient photocurrent compared with the bulk region as blocking region (shallow pink region). The thick film can be treated as a double-layer system with widths of $d_a$ and $d_b$ (Hu et al., 2010b). Due to the large thickness and an imbalance of carrier transport, space charges are accumulated in the active layer. The built-in electric field will be changed, which may lead to the generation of polarisation current in the film.

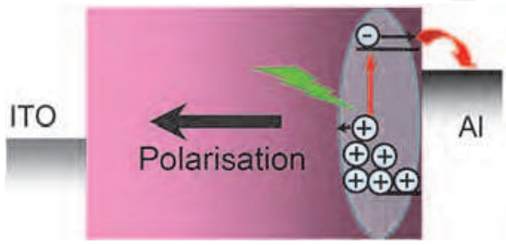


Fig. 9. A schematic view of BDTDA photocells.

### 3.1 Total current in a double-layer model

Theoretic analyses were performed to explore the mechanisms. To simplify the related theoretic analyses, electric fields in both regions are regarded as uniform and thus the BDTDA films can be separated into a double-layer film. Moreover, the thickness of both layers is assumed to be constant.

#### 3.1.1 Theoretic analyses for a double-layer model

Based on the total current equation (Guru & Hiziroğlu, 2004), the current density $j$ through the double layers is written as follows:

$$j = (\sigma_{b0} + \sigma_b) E_b(t) + \varepsilon_0 \varepsilon_b \frac{dE_b(t)}{dt} = (\sigma_{a0} + \sigma_a) E_a(t) + \varepsilon_0 \varepsilon_a \frac{dE_a(t)}{dt}, \quad (1)$$

where $\sigma_{b0}$, $\sigma_b$, $\varepsilon_b$, and $E_b(t)$ pertain to dark conductivity, photoconductivity, relative dielectric constant, and the time $t$ dependence of the uniform electric field, respectively, in the bulk blocking region. Meanwhile, $\sigma_{a0}$, $\sigma_a$, $\varepsilon_a$, and $E_a(t)$ express the corresponding quantities in the active junction region. The constant $\varepsilon_0$ denotes the dielectric constant of free space. The first terms in both sides of Eq. (1) are conduction current, while the second terms are displacement current. All parameters for conductivity are assumed to be time independent and dark conductivities were ignored. Taking the bias voltage ($V = E_b d_b + E_a d_a$) and the boundary condition $\varepsilon_b E_b(0) = \varepsilon_a E_a(0)$ into account, we can resolve Eq. (1), and the time dependence of $E_b$, $E_a$ and $j$ can be written as:

$$E_b(t) = \frac{\sigma_a V}{d_b \sigma_a + d_a \sigma_b} + \left( \frac{\varepsilon_a}{d_b \varepsilon_a + d_a \varepsilon_b} - \frac{\sigma_a}{d_b \sigma_a + d_a \sigma_b} \right) V e^{-t/\tau}, \quad (2a)$$

$$E_a(t) = \frac{\sigma_b V}{d_b\sigma_a + d_a\sigma_b} + \left( \frac{\varepsilon_b}{d_b\varepsilon_a + d_a\varepsilon_b} - \frac{\sigma_b}{d_b\sigma_a + d_a\sigma_b} \right) V e^{-t/\tau}, \tag{2b}$$

$$j = \frac{\sigma_b\sigma_a}{d_b\sigma_a + d_a\sigma_b} V + \frac{\left(\varepsilon_a\sigma_b - \varepsilon_b\sigma_a\right)^2 d_b d_a V}{\left(d_b\varepsilon_a + d_a\varepsilon_b\right)^2 \left(d_b\sigma_a + d_a\sigma_b\right)} e^{-t/\tau}, \tag{3}$$

where

$$\tau = \frac{\varepsilon_0\left(d_b\varepsilon_a + d_a\varepsilon_b\right)}{d_b\sigma_a + d_a\sigma_b}. \tag{4}$$

As shown in Eq. (4), the physics of decay time $\tau$ relates to the extraction speed for the free carriers by electrodes and dielectric property/polarisation in the films. Subsequently, we can estimate the total collected charges at time $t$ in the active side electrode, which is given by the following:

$$Q(t) = \int_0^t Aj(t)dt - \int_0^t i(t)dt, \tag{5}$$

where $i(t)$ is the discharging current in the external circuit. We take into account that the voltage drop across load resistor $R$ is equal to that across the photocell, particularly the following:

$$i(t)R = \frac{\int_0^t Aj(t)dt - \int_0^t i(t)dt}{C}, \tag{6}$$

where $C$ is the capacitance of the photocell. Since the initial current $i(0) = 0$, Eq. (6) can be resolved and the external discharging current $i(t)$ (i.e., anomalous transient photocurrent) is expressed as follows:

$$i(t) = \frac{S\xi_0}{\left(\tau - RC\right)}\left( e^{-\frac{t}{\tau}} - e^{-\frac{t}{RC}} \right) + S\zeta\left(1 - e^{-\frac{t}{RC}}\right), \tag{7}$$

where

$$\xi_0 = \frac{\varepsilon_0\left(\varepsilon_a\sigma_b - \varepsilon_b\sigma_a\right)^2 d_b d_a V}{\left(d_b\varepsilon_a + d_a\varepsilon_b\right)\left(d_b\sigma_a + d_a\sigma_b\right)^2}, \ \zeta = \frac{\sigma_b\sigma_a}{d_b\sigma_a + d_a\sigma_b} V$$

### 3.1.2 Simplified analyses for BDTDA photocells

In general, photogenerated excitons in organic materials can be dissociated only at donor-acceptor interfaces, or by a strong local electric field (Nicholson & Castro, 2010). If the film thickness is considerably larger tthan exciton diffusion length and carrier drift length, the excitons and carriers far from the electrodes cannot contribute to the photocurrent. In other words, the photoconductivity $\sigma_a$, which is proportional to carrier mobility $\mu$ and density $n$ in the junction (active region), is considerably larger than that in the bulk region, as well as the

dark conductivity. Therefore, other conductivities ($\sigma_{b0}$, $\sigma_b$, and $\sigma_{a0}$) can be ignored. Eqs. (2) and (7) can therefore be expressed as follows:

$$E_b(t) = \frac{V}{d_b} + \left( \frac{\varepsilon_a}{d_b\varepsilon_a + d_a\varepsilon_b} - \frac{1}{d_b} \right) V e^{-t/\tau}, \tag{8a}$$

$$E_a(t) = \frac{\varepsilon_b}{d_b\varepsilon_a + d_a\varepsilon_b} V e^{-t/\tau}, \tag{8b}$$

$$i(t) = \frac{S\xi}{(\tau - RC)} \left( e^{-\frac{t}{\tau}} - e^{-\frac{t}{RC}} \right) \tag{9}$$

with

$$\xi = \frac{\varepsilon_0 \varepsilon_b{}^2 d_a V}{(d_b\varepsilon_a + d_a\varepsilon_b) d_b} \tag{10}$$

and

$$\tau = \frac{\varepsilon_0 (d_b\varepsilon_a + d_a\varepsilon_b)}{d_b\sigma_a}. \tag{11}$$

Obviously, photogenerated carriers in the junction region that can be collected by electrodes will be exhausted if photoconductivity of the blocking region is extremely small. The space charge will be accumulated in the film and thus the electric field can be changed, as shown in Eq. (9). This naturally leads to a polarisation current. Two mechanisms, including $\tau$ and $RC$ time constant, are responsible for the decay of the anomalous transient photocurrent.
The derivative calculation was performed for Eq. (9), and a rise time $\tau_R$ can be obtained. In particular, after a time

$$t = \tau_R = \frac{RC\kappa}{RCI - \kappa} \ln \frac{RCI}{\kappa}, \tag{12}$$

with $\kappa = \tau I = \varepsilon_0(d_b\varepsilon_a + d_a\varepsilon_b)/d_b e a \mu$, the largest current density $J_m$ can be achieved, which is expressed as follows:

$$J_m = \frac{\xi}{(\tau - RC)} \left( \frac{RC}{\tau} \right)^{-\frac{RC}{RC-\tau}} \left( 1 - \frac{RC}{\tau} \right). \tag{13}$$

Since $\sigma_a = e\alpha I\mu$, where $a$ is quantum efficiency and $aI$ means carrier density with a light intensity of $I$, and $e$ means the elementary charge, the decay time $\tau$ can be written as follows:

$$\tau = \frac{\varepsilon_0 (d_b\varepsilon_a + d_a\varepsilon_b)}{e d_b \alpha I \mu}, \tag{14}$$

which suggests a relationship of $\tau \propto I^{-1}$. This relation fits the experimental data well. We consider the situation of a weak illumination, which will lead to a large τ. If $\tau >> RC$, the discharging current density in Eq. (9) will be

$$J \approx J_m e^{-\frac{t}{\tau}}, \tag{15}$$

with a maxima $J$(t) value $J_m$

$$J_m = \frac{d_a V e \alpha I \mu}{\left(d_b \varepsilon_a / \varepsilon_b + d_a\right)^2} \propto I \,. \tag{16}$$

Equation (15) suggests that the anomalous transient photocurrent exhibits exponential decay under weak irradiation and/or with a very small $RC$ time constant in the circuit, which fits well with the experimental behaviour in Fig. 7(a). It is notable that $J_m \propto \varepsilon_b^2$ in Eq. (16), indicating the effects from the dielectric constant of the bulk region. On the contrary, stronger illumination triggers a smaller $\tau$, which is related to the dielectric constants of the materials and photoconductivity in the junction region. If $\tau << RC$, the time constant in the circuits will dominate the decay, and shows resistance dependence as well as an exponential relationship.

### 3.2 Discussions

Both Eqs. (7) and (9) indicate that the anomalous transient photocurrent is a superposed signal with two mechanisms, namely, electron extraction from the junction region, and discharging process in the external circuit with a time constant of $RC$. It is clear that the thickness of our BDTDA films (300 nm) is excessively large, exceeding the exciton diffusion length and carrier drift length. Upon illumination, photogenerated electrons near the cathode are extracted as conduction current, while electrons on the other side cannot move across the thick film to compensate. This induces the transient conduction current.

The capacitance and dielectric constant in the equations involve polarization mainly in the bulk region triggered by photogenerated space charges in the films. The dielectric property of BDTDA strongly influences the anomalous transient photocurrent. Based on theoretic analyses, it is natural that the anomalous behaviour is universal for the thin films with large polarity, poor mobility and relatively large thickness. Though the carriers in organic materials cannot withstand a long trip due to various means of dissipation, including traps and recombination, displacement or a polarisation current can generate a large anomalous transient photocurrent without experiencing a long trip. Fast generation of this photocurrent is possible because the photoinduced polarisation current allows localised charges to oscillate around their equilibrium states. This is promising for high-speed organic photodetectors.

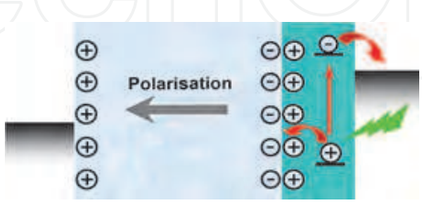


Fig. 10. A schematic display of an anode/ blocking layer /active layer/cathode photosensor.

## 4. Metal/insulator/semiconductor/metal type photocells

Based on the double-layer model, we developed a device to confirm the theoretic analyses in Section 3. A transparent thick organic insulator layer as a blocking layer was adopted to

substitute the bulk region in BDTDA photocells, and an organic semiconductor thin layer as an active layer was chosen to substitute the junction region. Figure 10 demonstrates the photocell with a structure of metal/organic insulator/organic semiconductor/metal, which may be utilised for light detection as well. The thickness of the semiconductor layer is targeted around 20 nm, which is equivalent to the carrier drift length. The organic double layers between the metals induce an imbalance of carrier transports; in particular, only one type of carrier can be collected by the electrodes. These will facilitate accumulation of the other type of carriers as space charges at the interface of the blocking layer and active layer. In this structure, the dielectric property of the insulator layer will strongly influence the signals.

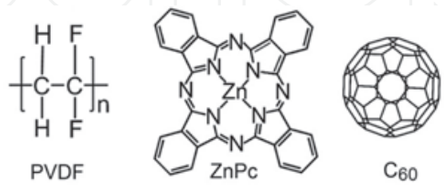


Fig. 11. Chemical structures of PVDF and ZnPc:$C_{60}$ donor-acceptor systems.

### 4.1 Photoresponses of ITO/PVDF/ZnPc:$C_{60}$/Al

To check the photoresponse of this kind of photocell, an equivalent metal/blocking layer/semiconductor layer/metal photocell was fabricated with ITO and Al electrodes. A well-known transparent polymer, polyvinylidene fluoride (PVDF, 8 wt% in dimethyl formamide), was adopted for the blocking layer and spin-coated onto a hot ITO glass slide (100 $^{o}$C). Thickness was estimated to be ~1 μm by cross-sectional SEM images. At the top of the blocking layer, a 30-nm active layer with a high charge-separation efficiency was prepared with zinc phthalocyanine (ZnPc) and fullerene ($C_{60}$) (molar ratio: 1:1, see Fig. 11 for their molecular structures) by co-deposition. Subsequently, the Al cathode was thermally evaporated onto the blend film. Photocurrent measurements were conducted under an illumination from a green laser (532 nm) controlled by a multifunction synthesiser. Photoresponses across a load resistor of $10^5$ Ω were recorded on an oscilloscope.

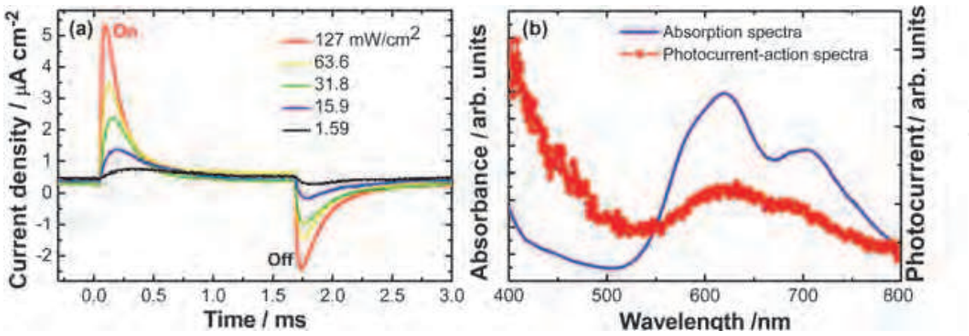


Fig. 12. (a) Photoresponses of an ITO/PVDF/ZnPc:$C_{60}$/Al photocell under an illumination of different intensities; (b) a comparison between the absorption spectra of the blend films (blue curve) and photocurrent-action spectra of the photocell (red curve).

#### 4.1.1 Photoresponses

Figure 12 shows the photoresponses with various light intensities. Upon laser illumination, a large anomalous transient photocurrent similar to that in the BDTDA photocells is

observed, and a negative anomalous transient photocurrent appears just after the illumination. Both the positive and negative anomalous transient photocurrent increase with increases in light intensity, and a faster decay can be obtained under a stronger illumination, which fits the expectation of Eq. (12). Absorption spectra of the blend films and photocurrent-action spectra (Fig. 12(b)) were collected for comparison. The peaks in these spectra are in agreement, indicating that the active layer does play a primary role in the production of this anomalous transient photocurrent. It is notable that no signals were obtained in the ITO/PVDF/Al structure, suggesting that only the active layer was the sensitive component. In addition, the relationship between anomalous transient photocurrent and weak light intensity was observed to exhibit linearity.

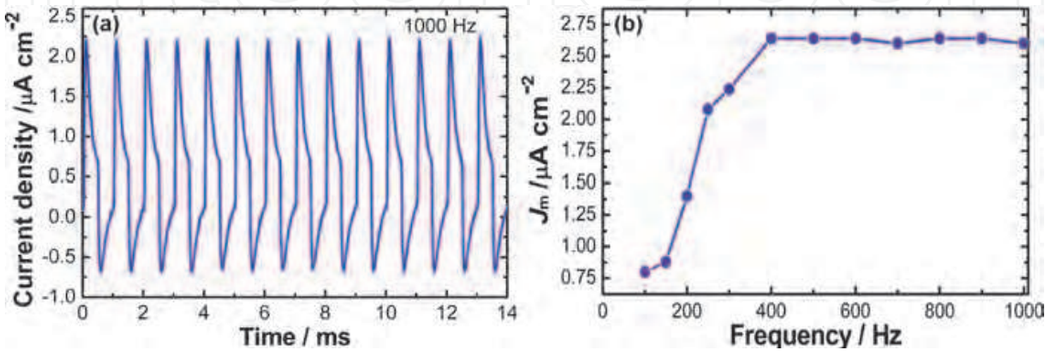


Fig. 13. (a) Photoresponses of an ITO/PVDF (1 μm)/ZnPc:$C_{60}$ (30 nm)/Al photocell with a light modulation of 1 kHz (31.8 mW/cm$^2$). (b) Frequency dependence of the photoresponses.

We examined the reproducibility of the anomalous transient photocurrent as well. Continuous current oscillation induced by frequency modulation is stably observed without degeneration (Fig. 13(a)). Evidently, the effective current will be increased as modulation frequency increases, as more current peaks can be generated in a fixed time period. It is notable that the values of the anomalous transient photocurrent peaks increase with increases in modulation frequency, and saturation is subsequently achieved after a certain modulation frequency, as shown in Fig. 13(b).

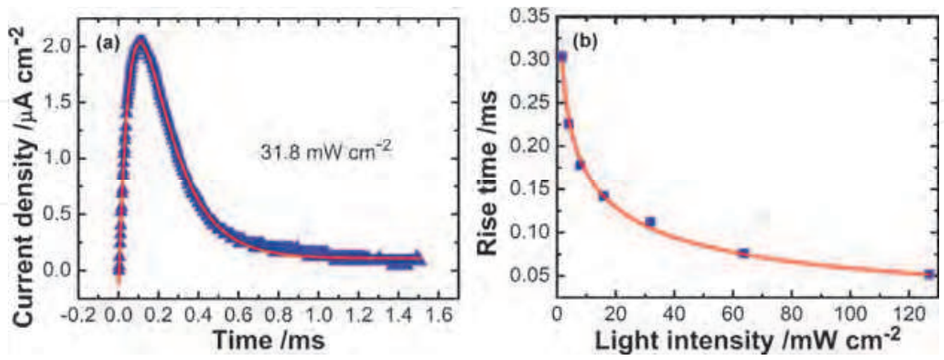


Fig. 14. (a) Simulations for the positive anomalous transient photocurrent based on (a) Eq. (7) and (b) Eq. (12) at 100 Hz.

### 4.1.2 Theoretic analyses for the transient photocurrent

We performed theoretic simulations for the anomalous transient photocurrent from the metal/blocking layer/semiconductor layer/metal photocells based on Eqs. (7) and (12), as

shown in Fig. 14. The blue triangles in Fig. 14(a) show the time dependence of the current density of positive anomalous transient photocurrent obtained under an illumination of 31.8 mW/cm$^2$. The solid red curve in this figure shows the theoretical simulations from Eq. (7). The *RC* time constant was extracted from the simulation to be $6.8\times10^{-5}$ s, which is considerably close to the experimental value ($4.2\times10^{-5}$ s, experimentally determined for the present circuit by an LCR meter at 100 Hz). $\tau$ was estimated to be ~$1.6\times10^{-4}$ s, during which 1-(1/e) of the photogenerated carriers that can be extracted will be collected by electrodes. The blue squares in Fig. 14(b) depict the dependence of the rise time $\tau_R$ on light intensity. This behaviour is reproduced by Eq. (12) (solid curve) as well. The *RC* time constant and $\tau$ are estimated to be $8.3\times10^{-5}$ s and $1.4\times10^{-4}$ s under an illumination of 31.8 mW/cm$^2$, respectively. Both simulated values from Eqs. (7) and (12) are in approximate agreement with each other, suggesting that the established double-layer model is reasonable for the explanation of anomalous transient photocurrent.

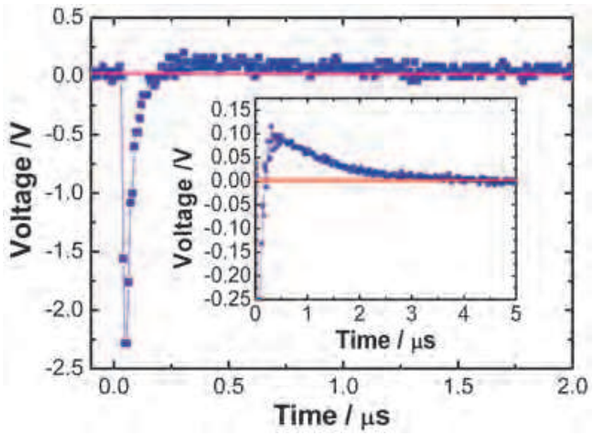


Fig. 15. Impulse response of the ITO/PVDF/ZnPc:$C_{60}$/Al photocell under a zero bias voltage; the inset is a magnified version of the recovery process.

### 4.1.3 Impulse response

To evaluate the lifetime of anomalous transient photocurrent, an impulse response was examined with a nanosecond laser beam (600 nm) from an optical parametric oscillator pumped by a Nd:YAG laser (10 Hz; pulse width: ~6 ns; power: ~1.08 μJ/pulse). A digital oscilloscope and a dc 300-MHz amplifier were used to collect voltage response with an input resistance of 50 Ω. A photocell with a structure of ITO/polystyrene (1 μm)/ZnPc:$C_{60}$ (20 nm)/Al was prepared for comparison with the ITO/PVDF (1 μm)/ZnPc:$C_{60}$ (20 nm)/Al photocells. The fabrication method for the polystyrene blocking layer was the same as that for PVDF.

Figure 15 shows the impulse response of the photocell with a PVDF blocking layer, which consists of rise, decay, and recovery processes. This behaviour is similar to that of the pyroelectric detectors with slower rise, decay, and recovery times (Odon, 2005; Polla et al., 1991), though their mechanisms are quite different. The *RC* constant in this circuit was estimated to be ~5 ns. Rise and decay time of the PVDF photocell can be observed as ~15 and 100 ns, respectively. Both the rise and decay times show an *RC* constant dependence; they increase along with increases in the *RC* constant (not shown). However, the recovery time exhibits a long time scale of ~2.5 μs (see inset of Fig. 15) and is independent of the *RC* constant.

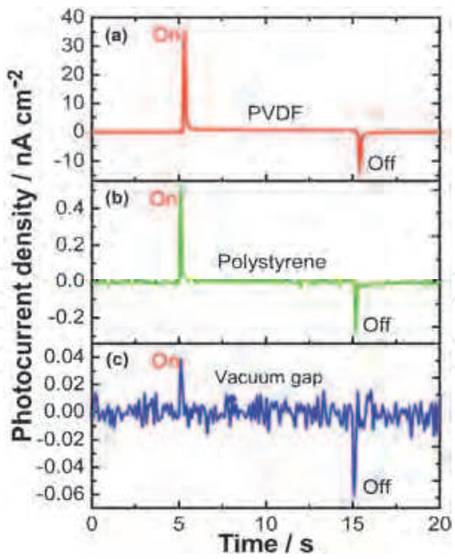


Fig. 16. Dielectric constant dependence of the anomalous transient photocurrent under an illumination (532 nm) of 160 mW/cm²; (a), (b) and (c) show the short-circuit anomalous transient photocurrent in the metal/blocking layer/semiconductor layer/metal photosensor with PVDF, polystyrene, and vacuum gap as blocking layers, respectively.

Faster response can be achieved by decreasing the dielectric constant ε of blocking layer. For example, substitution of the PVDF layer (ε ≈ 7-13) (Kerbow & Sperati, 1999) by polystyrene (ε ≈ 2.6) (Cullen & Yu, 1971) brings about a considerably faster rise (~5 ns) and decay (~8 ns) times at 0 V, but recover time remains to be ~1 μs. Slow recovery time could be ascribed to an energy barrier between the donor-acceptor and/or semiconductor-metal interfaces. Considering that the polarisation current is proportional to the variation rate of $E_b$ triggered by the photogenerated space charges, a faster generation of space charges by a sharper light pulse can bring about a larger anomalous transient photocurrent, even when only a small number of space charges are generated. Therefore, device speed is mainly determined by the rise and decay time, even though the system does not completely recover.

#### 4.1.4 Dielectric influences

We examined the relation between the dielectric constant $\varepsilon_b$ of the blocking layer and the quantum efficiency of anomalous transient photocurrent. Photocells with three different blocking layers (1 μm), namely, with vacuum gap ($\varepsilon$ = 1), polystyrene, and PVDF were prepared. Thickness of all the active layers is approximately 20 nm. Figure 16 demonstrates the short-circuit photoresponses of the three photocells against a strong illumination (160 mW/cm²). The values of the anomalous transient photocurrent dramatically increase with $\varepsilon_b$ as predicted in Eq. (16). As such, we can control the transient conversion efficiency by changing the $\varepsilon$ value of blocking layer. It is notable that the positive anomalous transient photocurrent of the PVDF photocell is ~8×10² times larger than that of the vacuum-gap photocell, though a rough estimation based on Eq. (16) suggests a difference of two orders of magnitude. The internal quantum efficiency of anomalous transient photocurrent in this PVDF cell under a weak illumination (0.2 μW/cm²; 560 nm) from a halogen lamp is calculated to be approximately 34% (root mean square, rms). The photoresponsivity at 560 nm (0.2 μW/cm²) reaches 10 mA/W (rms)

even without applying a bias voltage, which is comparable to those of conventional organic photodetectors operated by a bias voltage (Iwasaki et al., 2009; Narayan & Singh, 1999; O'Brien et al., 2006). It is believed that more charges stored in the PVDF photocell with a larger $\varepsilon$ were released upon illumination, when compared with the polystyrene and vaccum gap photocells.

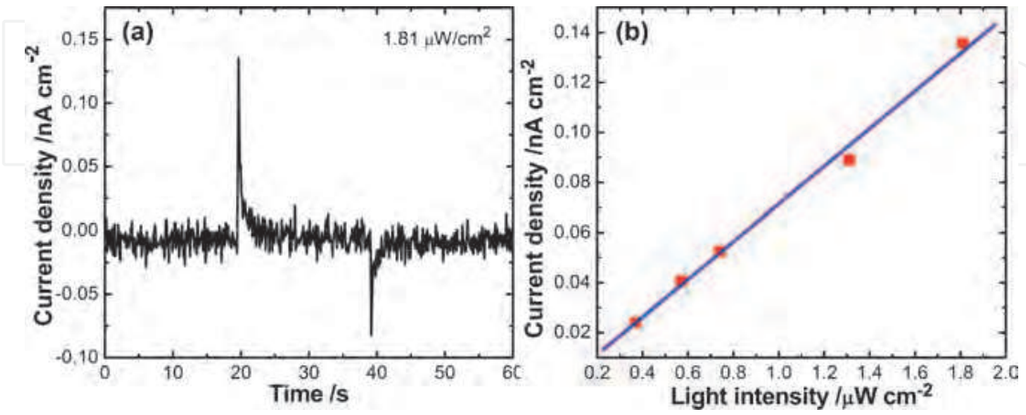


Fig. 17. (a) Photoresponse of ITO/ ZnPc/polystyrene (1 μm)/Al photocells under a zero bias voltage; (b) light intensity dependence of peak anomalous transient photocurrent value.

### 4.2 Photoconductivity dependence

Based on Eq. (14), decay time $\tau$ is inversely proportional to photoconductivity $\sigma_a = en\mu$, where $n = aI$ is the photogenerated free carrier density. Therefore, larger carrier mobility and density will induce faster decay and a larger signal if the $RC$ time constant in a circuit is very small. To check this relationship, ZnPc (30 nm) as the active layer was utilised in the metal/blocking layer/semiconductor layer/metal structure by thermal evaporation with a speed of 1 Å/s. Polystyrene layer (1 μm) by spin coating was adopted as the blocking layer. Two types of photocells with different structures for this material were produced, namely, ITO/polystyrene/ZnPc/Al and ITO/ZnPc/polystyrene/Al. As expected, the former does not exhibit signals since ZnPc is an excellent donor material. The latter shows a signal (see Fig. 17) and only holes are collected by the ITO electrode, which can be judged by the current direction. However, compared to those from the blend film (or bulk-heterojunction) devices, the signal from ZnPc photocells is considerably weaker due to a lower charge separation efficiency, which leads to a smaller carrier density. We likewise examined the light intensity dependence of anomalous transient photocurrent. As predicted in Section 3, intensity dependence of anomalous transient photocurrent does exhibit linearity (Fig. 17(b)) under weak illumination with a monomolecular or geminate recombination.

### 4.3 Discussions

Photoresponses from the metal/blocking layer/semiconductor layer/metal structure even with a vacuum gap is promising, indicating potential for pulse light detection. As we know, metal/semiconductor/metal type organic thin film device usually exhibits a large dark current due to pin holes, which leads to a small photocurrent. The employment of a blocking layer hampers the formation of pin holes and results in an extremely small dark current. It is possible now to utilise ultrathin films only with the highest internal quantum

efficiency for light detection. Compared with ideal metal/semiconductor/metal photocells with the same thickness in which conduction photocurrent $J_{ph}$ can be written as follows:

$$J_{ph} = \frac{Ve\alpha I\mu}{d_b + d_a}, \tag{17}$$

the metal/blocking layer/semiconductor layer/metal structure may exhibit a larger anomalous transient photocurrent current if we select an appropriate blocking layer and active layer with a small value of $d_b/d_a$, and small dielectric constant ratio ($\varepsilon_a/\varepsilon_b$). These can be judged from Eq. (16) [1]. Therefore, it is possible to release more stored charges in the capacitor type photocells upon illumination in addition to the photogenerated free carriers. Equation (14) likewise indicates a promising method for characterisation of carrier transport. As we can see from this equation, the anomalous transient photocurrent signal is related to carrier mobility and density. Therefore, mobility can be estimated if we extract the decay time $\tau$ from theoretic simulations, and obtain the photogenerated carrier density by other methods, such as light-induced electron paramagnetic resonance technique. In addition, we can utilise the metal/blocking layer/semiconductor layer/metal structure to determine the carrier type in an organic semiconductor, as described in Section 4.2.

## 5. Conclusion

In summary, we analysed the anomalous transient photocurrent in the BDTDA photocells based on a double-layer model. Resuts indicate that the dielectric property of organic materials will strongly influence the anomalous behaviour. For instance, a large dielectric constant will induce a larger anomalous photocurrent. This was confirmed in equivalent devices, such as ITO/PVDF or polystyrene/ZnPc:$C_{60}$/Al, in which the PVDF and polystyrene layer act as the bulk region, and the blend film acts as the junction region in the BDTDA photocells. Both theoretic and experimental results fit well with each other, suggesting that polarisation and fast extraction of photogenerated carriers in the blend film play significant roles in this behaviour. The theoretic analyses likewise indicate that the anomalous transient photocurrent may achieve a larger value if proper conditions are satisfied, compared to the conventional metal/semiconductor/metal photocells with the same total thickness. It is notable that the metal/blocking layer/semiconductor layer/metal structure is immune from pin-hole effects which usually exist in ultrathin conventional devices. Stored charges in the metal/blocking layer/semiconductor layer/metal capacitor photocells can be released upon illumination, which is quite different from the conventional principles for light detection or harvesting. These indicate potential optoelectronic conversion for pulse light detection in various fields, including communications, remote control, and image sensors. The obtained theory may also play a role in the characterisation of carrier transport along the directions perpendicular to the electrodes in the metal/blocking layer/semiconductor layer/metal photocells.

[1]For comparison, Eq. (16) can be changed to the following:

$$J_m = Ve\alpha I\mu / \left( d_a + 2d_b \varepsilon_a/\varepsilon_b + d_b^{\,2} \varepsilon_a^{\,2} / d_a^{\,2} \varepsilon_b^{\,2} \right).$$

## 6. Acknowledgments

The authors are indebted to Prof. Hiroshi Ito for his technical supports and constructive suggestions. Also acknowledged are the research group members who contributed to this work through useful discussions and provision of materials. This research was supported by a Grant-in-Aid for Scientific Research from the Ministry of Education, Culture, Sports, Science, and Technology (MEXT) and by CREST, JST. Dr. Hu also thanks the National Natural Science Foundation of China (No. 11004172 and 10804098) and the Zhejiang Provincial Natural Science Foundation of China (No. Y607472).

## 7. References

Andriesh, A. M. *et al.* (1983), Anomalous Transient Photocurrent in Disordered Semiconductors - Theory and Experiment. *Solid State Communications*, Vol. 48, No. 12, pp. 1041-1043, ISSN 0038-1098.

Binet, F. *et al.* (1996), Mechanisms of recombination in GaN photodetectors. *Applied Physics Letters*, Vol. 69, No. 9, pp. 1202-1204, ISSN 0003-6951.

Blanchet, G. B. *et al.* (2003), Large area, high resolution, dry printing of conducting polymers for organic electronics. *Applied Physics Letters*, Vol. 82, No. 3, pp. 463-465, ISSN 0003-6951.

Blom, P. W. M. *et al.* (1997), Electric-field and temperature dependence of the hole mobility in poly(p-phenylene vinylene). *Physical Review B*, Vol. 55, No. 2, pp. R656-R659, ISSN 0163-1829.

Bryan, C. D. *et al.* (1996), Preparation and characterization of the disjoint diradical 4,4'-bis(1,2,3,5-dithiadiazolyl) [$S_2N_2C$-$CN_2S_2$] and its iodine charge transfer salt [$S_2N_2C$-$CN_2S_2$]. *Journal of the American Chemical Society*, Vol. 118, No. 2, pp. 330-338, ISSN 0002-7863.

Chakraborty, A. K. & Mallik, B. (2009), Photoinduced anomalous current changes in some organometallic materials. *Current Applied Physics*, Vol. 9, No. 5, pp. 1079-1087, ISSN 1567-1739.

Coropceanu, V. *et al.* (2007), Charge transport in organic semiconductors. *Chemical Reviews*, Vol. 107, No. 4, pp. 926-952, ISSN 0009-2665.

Cullen, A. L. & Yu, P. K. (1971), Accurate Measurement of Permittivity by Means of an Open Resonator. *Proceedings of the Royal Society of London Series a-Mathematical and Physical Sciences*, Vol. 325, No. 1563, pp. 493-509, ISSN 0950–1207

Forrest, S. R. & Thompson, M. E. (2007), Introduction: Organic electronics and optoelectronics. *Chemical Reviews*, Vol. 107, No. 4, pp. 923-925, ISSN 0009-2665.

Gunes, S. *et al.* (2007), Conjugated polymer-based organic solar cells. *Chemical Reviews*, Vol. 107, No. 4, pp. 1324-1338, ISSN 0009-2665.

Guru, B. S. & Hiziroğlu, H. R. (2004), *Electromagnetic Field Theory Fundamentals*, Cambridge Univ. Press, Cambridge. ISBN 0521830168.

Hamilton, M. C. & Kanicki, J. (2004), Organic polymer thin-film transistor photosensors. *Ieee Journal of Selected Topics in Quantum Electronics*, Vol. 10, No. 4, pp. 840-848, ISSN 1077-260X.

Hu, L. G. *et al.* (2010), Highly efficient alternating photocurrent from interactive organic-radical dimers: A novel light-harvesting mechanism for optoelectronic conversion. *Chemical Physics Letters*, Vol. 484, No. 4-6, pp. 177-180, ISSN 0009-2614.

Hu, L. G. *et al.* (2010), Optoelectronic conversion by polarization current, triggered by space charges at organic-based interfaces. *Applied Physics Letters*, Vol. 96, No. 24, pp. 243303, ISSN 0003-6951.

Ito, H. *et al.* (2008), Photocurrent of regioregular poly(3-alkylthiophene)/fullerene composites in surface-type photocells. *Thin Solid Films*, Vol. 516, No. 9, pp. 2743-2746, ISSN 0040-6090.

Iwamoto, M. (1996), Transient current across insulating films with long-range movements of charge carriers. *Journal of Applied Physics*, Vol. 79, No. 10, pp. 7936-7943, ISSN 0021-8979.

Iwasaki, A. *et al.* (2009), Interactive Radical Dimers in Photoconductive Organic Thin Films. *Angewandte Chemie-International Edition*, Vol. 48, No. 22, pp. 4022-4024, ISSN 1433-7851.

Kao, K.-C. (2004), *Dielectric Phenomena in Solids* Elsevier Academic Press, Amsterdam. ISBN 978-0-12-396561-5.

Karl, N. (2003), Charge carrier transport in organic semiconductors. *Synthetic Metals*, Vol. 133, No. pp. 649-657, ISSN 0379-6779.

Kumar, A. *et al.* (1987), Anomalous Decay of Photocurrent in Amorphous Thin-Films of $Ge_{22}Se_{78}$. *Physical Review B*, Vol. 35, No. 11, pp. 5635-5638, ISSN 0163-1829.

Marumoto, K. *et al.* (2004), Quadrimolecular recombination kinetics of photogenerated charge carriers in regioregular poly (3-alkylthiophene) / fullerene composites. *Applied Physics Letters*, Vol. 84, No. 8, pp. 1317-1319, ISSN 0003-6951.

Mihailetchi, V. D. *et al.* (2005), Space-charge limited photocurrent. *Physical Review Letters*, Vol. 94, No. 12, pp. 126602, ISSN 0031-9007.

Narayan, K. S. & Singh, T. B. (1999), Nanocrystalline titanium dioxide-dispersed semiconducting polymer photodetectors. *Applied Physics Letters*, Vol. 74, No. 23, pp. 3456-3458, ISSN 0003-6951.

Nicholson, P. G. & Castro, F. A. (2010), Organic photovoltaics: principles and techniques for nanometre scale characterization. *Nanotechnology*, Vol. 21, No. 49, pp. 492001, ISSN 0957-4484.

O'Brien, G. A. *et al.* (2006), A single polymer nanowire photodetector. *Advanced Materials*, Vol. 18, No. 18, pp. 2379-2383, ISSN 0935-9648.

Odon, A. (2005), Voltage Response of Pyroelectric PVDF Detector to Pulse Source of Optical Radiation. *Measurement Science Review*, Vol. 5, No. pp. 55-58, ISSN 1335-8871

Pandey, A. K. *et al.* (2008), Size effect on organic optoelectronics devices: Example of photovoltaic cell efficiency. *Physics Letters A*, Vol. 372, No. 8, pp. 1333-1336, ISSN 0375-9601.

Pettersson, L. A. A. *et al.* (2001), Quantum efficiency of exciton-to-charge generation in organic photovoltaic devices. *Journal of Applied Physics*, Vol. 89, No. 10, pp. 5564-5569, ISSN 0021-8979.

Polla, D. L. *et al.* (1991), Surface-Micromachined Pbtio3 Pyroelectric Detectors. *Applied Physics Letters*, Vol. 59, No. 27, pp. 3539-3541, ISSN 0003-6951.

Saragi, T. P. I. *et al.* (2007), Spiro compounds for organic optoelectronics. *Chemical Reviews*, Vol. 107, No. 4, pp. 1011-1065, ISSN 0009-2665.

Sharma, G. D. (1995), Electrical and photoelectrical properties of Schottky barrier devices using the chloro aluminium phthalocyanines. *Synthetic Metals*, Vol. 74, No. 3, pp. 227-234, ISSN 0379-6779.

Slooff, L. H. *et al.* (2007), Determining the internal quantum efficiency of highly efficient polymer solar cells through optical modeling. *Applied Physics Letters*, Vol. 90, No. 14, pp. 143506, ISSN 0003-6951.

Spanggaard, H. & Krebs, F. C. (2004), A brief history of the development of organic and polymeric photovoltaics. *Solar Energy Materials and Solar Cells*, Vol. 83, No. 2-3, pp. 125-146, ISSN 0927-0248.

Sugimura, A. *et al.* (1989), Anomalous Photoinduced Current Transients in Nematic Liquid-Crystals. *Physical Review Letters*, Vol. 63, No. 5, pp. 555-557, ISSN 0031-9007.

Tahira, K.&Kao, K. C. (1985), Anomalous Photocurrent Transient in Polyethylene. *Journal of Physics D-Applied Physics*, Vol. 18, No. 11, pp. 2247-2259, ISSN 0022-3727.

van Duren, J. K. J. *et al.* (2003), Injection-limited electron current in a methano-fullerene. *Journal of Applied Physics*, Vol. 94, No. 7, pp. 4477-4479, ISSN 0021-8979.

Wagner, R. E. & Mandelis, A. (1996), Nonlinear photothermal modulated optical reflectance and photocurrent phenomena in crystalline semiconductors .1. Theoretical. *Semiconductor Science and Technology*, Vol. 11, No. 3, pp. 289-299, ISSN 0268-1242.

Xu, Y. F. *et al.* (2004), Photoresponsivity of polymer thin-film transistors based on polyphenyleneethynylene derivative with improved hole injection. *Applied Physics Letters*, Vol. 85, No. 18, pp. 4219-4221, ISSN 0003-6951.

Xue, J. G. (2010), Perspectives on Organic Photovoltaics. *Polymer Reviews*, Vol. 50, No. 4, pp. 411-419, ISSN 1558-3724.

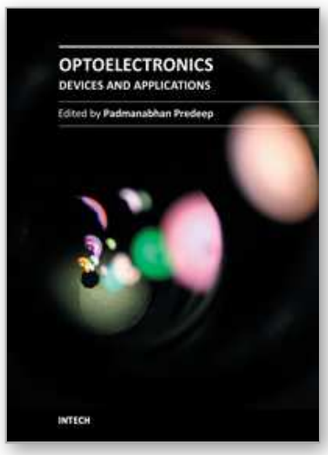


**Optoelectronics - Devices and Applications**

Edited by Prof. P. Predeep

ISBN 978-953-307-576-1
Hard cover, 630 pages
**Publisher** InTech
**Published online** 03, October, 2011
**Published in print edition** October, 2011

Optoelectronics - Devices and Applications is the second part of an edited anthology on the multifaced areas of optoelectronics by a selected group of authors including promising novices to experts in the field. Photonics and optoelectronics are making an impact multiple times as the semiconductor revolution made on the quality of our life. In telecommunication, entertainment devices, computational techniques, clean energy harvesting, medical instrumentation, materials and device characterization and scores of other areas of R&D the science of optics and electronics get coupled by fine technology advances to make incredibly large strides. The technology of light has advanced to a stage where disciplines sans boundaries are finding it indispensable. New design concepts are fast emerging and being tested and applications developed in an unimaginable pace and speed. The wide spectrum of topics related to optoelectronics and photonics presented here is sure to make this collection of essays extremely useful to students and other stake holders in the field such as researchers and device designers.



INTECH
open science | open minds

**InTech Europe**
University Campus STeP Ri
Slavka Krautzeka 83/A
51000 Rijeka, Croatia
Phone: +385 (51) 770 447
Fax: +385 (51) 686 166
www.intechopen.com

**InTech China**
Unit 405, Office Block, Hotel Equatorial Shanghai
No.65, Yan An Road (West), Shanghai, 200040, China
中国上海市延安西路65号上海国际贵都大饭店办公楼405单元
Phone: +86-21-62489820
Fax: +86-21-62489821

IntechOpen